One-Shot Blind Channel Estimation for OFDM Systems Over Frequency-Selective Fading Channels

A. Saci, *Student Member, IEEE*, A. Al-Dweik, *Senior Member, IEEE*, A. Shami, *Senior Member, IEEE*, and Y. Iraqi, *Senior Member, IEEE*

***Abstract*—This paper presents a blind channel estimation technique for orthogonal frequency division multiplexing (OFDM) communications systems. The proposed system is based on modulating particular pairs of subcarriers using amplitude shift keying (ASK) and phase shift keying (PSK), which enables the realization of a decision-directed (DD) one-shot blind channel estimator (OSBCE), with complexity and accuracy that are comparable to pilot-based channel estimation techniques. The performance of the proposed estimator is evaluated in terms of the mean squared error (MSE), where an accurate analytical expression is derived and verified using Monte Carlo simulation under various channel conditions. The obtained results show that the MSE of the proposed OSBCE is comparable to pilot-based estimators, which confirms the efficiency of the proposed OSBCE.**

***Index Terms*—Channel estimation, OFDM, mean squared error, frequency-selective fading, error rate analysis.**

I. Introduction

ORTHOGONAL frequency division multiplexing (OFDM) is a multicarrier modulation technique that received tremendous interest from the industry and academia over the past decade. The catalyst for such interest, is the special features that OFDM has, such as spectral efficiency, immunity to multipath propagation, efficient implementation using the fast Fourier transform (FFT) pairs, and low-complexity equalization [1]. Therefore, OFDM is currently adopted by several commercial standards, such as the second generation digital video broadcasting-terrestrial (DVB-T2) [2], wireless local area networks (WLAN) IEEE 802.11 [3], Worldwide Interoperability for Microwave Access (WiMAX) [4] and Long Term Evolution Advanced (LTE-A) [5]. Moreover, OFDM is a strong candidate for the upcoming fifth-generation (5G) wireless communications standard [6].

Acquiring the knowledge of channel state information (CSI), commonly known as channel estimation (CE), and channel equalization are two fundamental tasks that a receiver has to perform prior to information symbols extraction from the received signal. Generally speaking, most CE techniques reported in the literature can be classified based on their spectral efficiency, estimation accuracy, computational complexity, or the required observation window size. An efficient estimator is the one that can maximize the accuracy and spectral efficiency, while minimizing the complexity and observation window size. However, achieving all such conflicting objectives into one single design is generally infeasible, and hence, the system designer has to compromise some of these objectives based on the available system resources and quality of service (QoS) requirements. For most practical applications, a reasonable compromise can be achieved by using training symbols, where CSI is estimated at the receiver side by modulating particular subcarriers at the transmitter side using known symbols, denoted as reference or pilot symbols, and then, use such pilots for CE purposes [7]-[14]. In LTE-A [5], comb-type pilots are deployed in a time-frequency subcarrier grid as shown in Fig. 1a, where the pilots occupy about 4.7% of the total number of subcarriers. The spectral efficiency can be even lower for some other systems, such as the IEEE 802.11n, where pilot symbols constitute 7.1% of the total subcarriers. Moreover, in communications systems that involve burst transmission, such as frequency hopping and cognitive radio, the channel coefficients over consecutive OFDM symbols can be uncorrelated, and hence, pilot symbols are needed in every OFDM symbol, which degrades the spectral efficiency even further. Therefore, many algorithms have been proposed to estimate the CSI blindly, by utilizing only the received data symbols [15]-[25], and consequently, improve the spectral efficiency.

In the literature, blind CE is one of the widely addressed issues in wireless communications [8]-[26]. However, the problem remains open because, to the best of our knowledge, none of the techniques reported in the literature managed to resolve the conflicting objectives problem perfectly. For example, several blind estimators are designed based on the assumption that all subcarriers should be modulated using a constant modulus (CM) constellation, such as M-ary phase shift keying (MPSK) [16]-[19]. Although such techniques do not require pilot symbols, they indirectly degrade the spectral efficiency of the system because they prohibit using spectrally efficient modulation schemes, such as quadrature amplitude modulation (QAM). Therefore, it would be more factual to denote such techniques as conditionally-blind, to distinguish them from fully blind (FB) systems, which do not require pilot symbols and do not have any constraints on the modulation type or order. It is worth noting that conditionally-blind systems are different from semi-blind systems, in which the CE is performed using both, the pilot and data symbols

This work is sponsored by the ICT Fund, grant no. 11/15/TRA-ICTFund/KU.

A. Saci, A. Al-Dweik and A. Shami are with the Department of Electrical and Computer Engineering, Western University, London, ON, Canada (e-mail: {asaci, aaldweik, ashami2}@uwo.ca).

A. Al-Dweik is also with the Department of Electrical and Computer Engineering, Khalifa University, Abu Dhabi, UAE (e-mail: dweik@kustar.ac.ae).

Y. Iraqi is with the Department of Electrical and Computer Engineering, Khalifa University, Abu Dhabi, UAE (e-mail: youssef.iraqi@kustar.ac.ae).

This article has been accepted for publication in a future issue of this journal, but has not been fully edited. Content may change prior to final publication. Citation information: DOI 10.1109/TCOMM.2017.2740925, IEEE Transactions on Communications

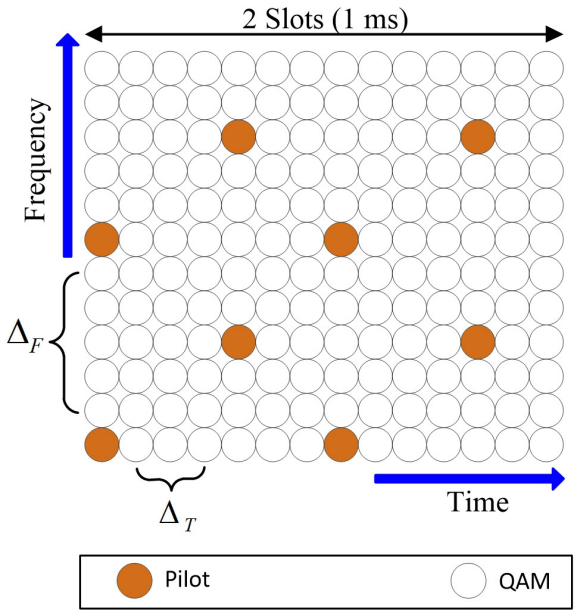

(a) LTE-A transmission grid.

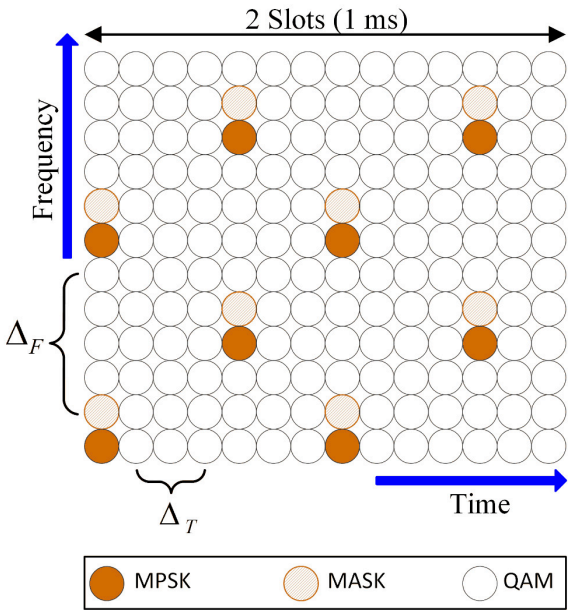

(b) OSBCE transmission grid.

Fig. 1. Time-frequency grid of LTE-A and the proposed OSBCE.

[24]-[26].

Computational complexity is another critical performance indicator used to compare various channel estimation techniques. Generally speaking, blind estimation techniques have higher computational complexity than pilot-based techniques [12], [21]. The excessive computational complexity is mainly caused by the iterative structure of such algorithms [21]-[23], or due to the requirements to perform an extensive search over the solution space [20]. Although the complexity of the system reported in [20] becomes comparable to pilot-based estimation at high signal-to-noise ratios (SNRs), such condition can be frequently violated in practical scenarios.

The observation window size specifies the number of OFDM symbols required to compute the CSI estimates. In CE techniques that require large observation window, the channel is assumed to be fixed over the observation period [16], [17], [19], [21]. Although such assumption is acceptable for static and slow fading channels, it is not actually the case for fast fading channels. Moreover, if the observation window size is very large, then such assumption becomes realizable only for static channels. Channel estimators that can perform CE within one OFDM block, denoted as one-shot estimators, usually outperform other estimators with multiple-symbols observation window [20].

The accuracy of CE techniques is typically evaluated using mean squared error (MSE), which is supposed to be sufficiently low to minimize the bit error rate (BER) degradation caused by CE errors [27]. In the literature, the performance of pilot-based CE is commonly used as a benchmark for comparison [7], [18], [27], because pilot-based estimation techniques offer reliable estimates and their impact on the BER is tolerable.

As it can be noted from the aforementioned discussion, pilot-based estimators have several attractive features in terms of complexity, estimation accuracy, and observation window size. However, the spectral efficiency remains the major concern. Practically speaking, the dominant standards such as DVB-T2 [2], WiMAX [4] and LTE-A [5], are using pilot-based CE, which implies that systems' designers prefer to compromise the spectral efficiency, but gain the other advantages. Unlike most of the work reported in the literature, this work presents a novel one-shot blind channel estimation (OSBCE) technique which is conditionally-blind, but only a small fraction of the subcarriers have the modulation-type constraint, and hence, it is spectrally efficient. The OSBCE is based on replacing the pilot symbols in conventional pilot-based systems with MPSK symbols, and the modulation type of the adjacent subcarriers is limited to M-ary amplitude shift keying (MASK) modulation. Such configuration allows detecting the MPSK symbols coherently using the partial channel information embedded in the MASK symbols. Then, the detected MPSK symbols are used to obtain the full channel information in a decision-directed (DD) manner. The complexity, observation window and accuracy of the OSBCE are comparable to pilot-based estimators while the spectral efficiency of the OSBCE is higher than pilot systems at moderate and high SNRs. The system performance is evaluated in terms of the symbol error rate (SER) and MSE, where a closed-form formula is derived for the SER while the MSE can be efficiently evaluated numerically. The obtained analytical results are confirmed using Monte Carlo simulation.

The rest of the paper is organized as follows. OFDM system and channel models are presented in Section II. The OSBCE model is introduced in Section III. Sections IV and V present the derivation of the SER and MSE, respectively. Spectral efficiency analysis is presented in Section VI. The numerical results are discussed in Section VII, and finally, the conclusion of the paper is drawn in Section VIII.

The notation used in the paper is as follows. Uppercase boldface letters such as $\mathbf{H}$ will denote $N \times N$ matrices, whereas lowercase boldface letters such as $\mathbf{x}$ will denote row or column vectors with N elements. Calligraphic letters with a hat such as $\hat{\mathcal{A}}$ will denote initial estimates of the variable A, while a regular symbol with a hat such as $\hat{A}$ will denote the final estimate of A. Blackboard symbols with the subscript such as $\mathbb{M}_Q$ will denote the set $\{0, 1, \ldots, M_Q - 1\}$. The Euclidean norm is denoted as $\|.\|$, and the operators ' $|$ ' and ' $\imath$ ' will denote the conditioning operation, interchangeably. Furthermore, $E\{\cdot\}$ denotes the expectation process, the complex conjugate, transpose, and Hermitian transpose will be denoted as $(\cdot)^*$, $(\cdot)^T$ and $(\cdot)^H$, respectively.

II. OFDM System and Channel Models

Consider an OFDM system with N subcarriers modulated by a sequence of N complex data symbols $\mathbf{a} = [A_0,\ A_1,\ ....,\ A_{N-1}]^T$. The data symbols are selected uniformly from a general constellation such as MPSK, QAM or MASK, with modulation orders M_P , M_Q and M_A, respectively. In pilot-based practical OFDM systems [5], N_P of the subcarriers are reserved for pilot symbols, which can be used for channel estimation and synchronization purposes. For the purpose of this work, we define three sets of indices for the subcarriers, namely,the set of pilots' indices $\mathbb{V} = \{v_1, v_2, \ldots, v_{N_P}\}$, the set of subcarriers' indices adjacent to the pilots $\mathbb{T} = \{t_1, t_2, \ldots, t_{N_P}\}$, and the set of indices of the remaining data symbols is denoted as $\mathbb{U}$. It is worth noting that the three sets are disjoint, $\mathbb{V} \cap \mathbb{T} \cap \mathbb{U}$, and $t_i = v_i + 1$.

The modulation process can be implemented efficiently using N-point inverse FFT (IFFT). The output of the IFFT process during the ℓth OFDM block is given by $\mathbf{x}(\ell) = \mathbf{F}^H \mathbf{a}(\ell)$, where $\mathbf{F}$ is the normalized $N \times N$ FFT matrix, and hence, $\mathbf{F}^H$ is the IFFT matrix. The elements of $\mathbf{F}^H$ are defined as $F_{i,k} = (1/\sqrt{N})e^{j2\pi ik/N}$ where i and k denote the row and column indices $i,\ k \in \{0, 1, ..., N-1\}$, respectively. For convenience, we drop the block index notation ℓ in the remaining parts unless it is necessary to include it. To eliminate inter-symbol-interference (ISI) between consecutive OFDM symbols and maintain the subcarriers' orthogonality in frequency-selective multipath fading channels, a cyclic prefix (CP) of length N_{CP} samples no less than the channel maximum delay spread (L_{h}) is formed by copying the last N_{CP} samples of $\mathbf{x}$ and appending them in front of the IFFT output to compose the OFDM symbol with a total length $N_{\mathrm{t}} = N + N_{\mathrm{CP}}$ samples and a duration of T_{t} seconds. Then, the complex baseband OFDM symbol during the ℓth signaling period $\tilde{\mathbf{x}}$ is upsampled, filtered and up-converted to a radio frequency centered at f_{c} before transmission through the antenna.

At the receiver front-end, the received signal is down-converted to baseband and sampled at a rate $T_{\mathrm{s}} = T_{\mathrm{t}}/N_{\mathrm{t}}$. In this work, we assume that the channel is composed of $L_{\mathrm{h}} + 1$ independent multipath components each of which has a gain $h_m \sim \mathcal{CN}\left(0, 2\sigma^2_{h_m}\right)$ and delay $m \times T_{\mathrm{s}}$, where $m \in \{0,\ 1,...,\ L_{\mathrm{h}}\}$. The channel taps are assumed to be constant over one OFDM symbol, but they may change over two consecutive symbols, which corresponds to a quasi-static multipath channel [28]. Then, the received signal after discarding the first N_{CP} CP samples, and computing the FFT can be expressed as,

$$\mathbf{r} = \mathbf{H}\mathbf{a} + \mathbf{w} \tag{1}$$

where $\mathbf{r} \in \mathbb{C}^{N\times 1}$,$\mathbf{w}$ denotes the additive white gaussian noise (AWGN) vector, whose samples are independent and identically distributed (i.i.d.) $w_k \sim \mathcal{CN}\left(0, 2\sigma^2_w\right)$, and $\mathbf{H}$ denotes the channel frequency response (CFR), which is defined as,

$$\mathbf{H} = \mathrm{diag}\left\{[H_0,\ H_1, \ldots,\ H_{N-1}]\right\} \tag{2}$$

where $H_k = \sum_{m=0}^{L_{\mathrm{h}}} h_m e^{-j2\pi mk/N}$.

It is worth noting that the diagonal elements of $\mathbf{H}$ are highly correlated, particularly the adjacent elements where the correlation coefficient $\varrho \triangleq E\{H_k H^*_{k+1}\}$ is defined as

$$\varrho = E\left\{\sum_{n=0}^{L_{\mathrm{h}}}\sum_{m=0}^{L_{\mathrm{h}}} h_n h^*_m e^{j2\pi\frac{-(n-m)k+n}{N}}\right\}. \tag{3}$$

Given that h_m and h_n are mutually independent $\forall m \neq n$, then $E\left\{|h_n|^2\right\} = 2\sigma^2_{h_n}$ and $E\{h_n h^*_m\}\,|_{n\neq m} = 0$. Thus

$$\varrho = \sum_{n=0}^{L_{\mathrm{h}}} \sigma^2_{h_n}\ e^{j2\pi\frac{n}{N}}. \tag{4}$$

The elements of the FFT output are then fed to a single-tap zero-forcing (ZF) or minimum mean squared error (MMSE) equalizer, followed by a maximum likelihood detector (MLD). In this work we consider the ZF equalizer, and hence, the estimated kth symbol can be expressed as

$$\hat{A}_k = \arg\min_{A^{(i)}_k, i\in\mathbb{M}_Q} \left|\frac{\hat{H}^*_k}{|\hat{H}_k|^2} r_k - A^{(i)}_k\right|^2,\ k \notin \mathbb{V} \tag{5}$$

where $\hat{H}_k$ is the estimated CFR at the kth subcarrier, $A^{(i)}_k$ are the trial values of the data symbols. It is worth noting that single-tap frequency-domain ZF and MMSE equalizers offer approximately the same performance in quasi-static single-input single-output (SISO) systems [29], [30]. However, the mathematical analysis of the MMSE equalizer is more intractable.

In OFDM-based systems such as LTE-A, the data symbols are arranged in a time-frequency grid as shown in Fig. 1a, and channel estimation based on such structure is typically performed over two steps. First, initial channel estimates are obtained at the positions of pilot symbols using least square estimation (LSE),

$$\hat{\mathcal{H}}_k = \frac{r_k}{A_k},\ k \in \mathbb{V} \tag{6}$$

where the pilot symbols values are assumed to be known at the receiver side. By noting that $r_k = H_k A_k + w_k$, the CFR estimates can be written as

$$\hat{\mathcal{H}}_k = H_k + q_k \tag{7}$$

where $H_k \sim \mathcal{CN}\left(0,\ 2\sigma^2_H\right)$ and $q_k \sim \mathcal{CN}\left(0,\ \frac{2\sigma^2_w}{|A_k|^2}\right)$.

Once the initial CFR $\hat{\mathcal{H}}_k\ \forall k \in \mathbb{V}$ is obtained, the CFR $\hat{H}_k(\ell)\ \forall k, \ell$ can be obtained as well given that the pilot grid density satisfies the two-dimensional (2-D) sampling theorem.

TABLE I
CORRELATION COEFFICIENT ϱ FOR COMMON CHANNEL MODELS ($N = 256$).

Channel model	Channel Profile	$\lvert\varrho\rvert$	$\arg\{\varrho\}$
cost207RAx4	Rural Area (RAx), 4 taps	0.99998	0.00169
cost207TUx6	Typical Urban (TUx), 6 taps	0.99475	0.05616
cost207TUx12	Typical Urban (TUx), 12 taps	0.99556	0.07981
cost207BUx6	Bad Urban (BUx), 6 taps	0.97447	0.19145

Then, optimal interpolation using a 2-D Wiener filter that exploits the time and frequency correlation of the channel can be invoked at the expense of substantial implementation complexity [31]. The complexity can be reduced by decomposing the 2-D interpolation process into two cascaded one dimensional (1-D) processes, and then use less computationally involved interpolation schemes [32], [33]. The channel estimation in 1-D can be obtained using various techniques such as linear interpolation [12], parametric estimation [34], or least-square-fitting [35]. It is worth noting that when nonlinear interpolation is invoked, the initial channel estimates at the pilots positions $\hat{\mathcal{H}}_k$ will be replaced by new estimates obtained from the fitting polynomial, and thus $\hat{H}_k \neq \hat{\mathcal{H}}_k$ [35]. Furthermore, in the special case where A_k belongs to CM constellation, it is sufficient to know the phase of the CFR to perform coherent MLD, which can be expressed as

$$\hat{A}_k = \arg \min_{A_k^{(i)},\, i \in \mathbb{M}_P} \left| e^{-j\hat{\theta}_k}\, r_k - A_k^{(i)} \right|^2 \tag{8}$$

where $\hat{\theta}_k \triangleq \arg\left\{\hat{H}_k\right\}$ is the estimated version of $\theta_k \triangleq \arg\{H_k\}$.

III. THE PROPOSED OSBCE

For most practical channel models, as indicated in Table I, it can be noted that $|\varrho| \approx 1$ and $\arg\{\varrho\} \approx 0$, which implies that $H_k \approx H_{k+1}$. Therefore, the FFT output at subcarriers k and k+1 can be written as

$$r_k = H_k A_k + w_k \tag{9}$$

and

$$r_{k+1} \approx H_k A_{k+1} + w_{k+1}. \tag{10}$$

Moreover, the AWGN at high SNRs can be ignored, and hence (10) can be further simplified to $r_{k+1} \approx H_k A_{k+1}$. Consequently, by carefully choosing the modulation types for the data symbols A_k and A_{k+1}, the information symbol A_k can be recovered blindly without explicit knowledge of H_k. Towards this goal, consider the case where A_{k+1} is modulated using unipolar MASK, $A_{k+1} \in \mathbb{R}^+$, the set of positive real numbers excluding zero, and A_k is modulated using MPSK. Consequently, MLD of A_k requires only the knowledge of $\hat{\theta}_k$, which can be obtained by noting that $\arg\{r_{k+1}\} \triangleq \hat{\vartheta}_{k+1} \approx \theta_k$. Therefore, the preliminary estimate of the CFR phase $\hat{\vartheta}_{k+1}$ can be used to obtain a preliminary estimate of the symbol A_k, where

$$\hat{\mathcal{A}}_k = \arg \min_{A_k^{(i)},\, i \in \mathbb{M}_P} \left| e^{-j\hat{\vartheta}_{k+1}}\, r_k - A_k^{(i)} \right|^2. \tag{11}$$

Furthermore, because $A_{k+1} \in \mathbb{R}^+$ and A_k has CM, the MLD in (11) can be also implemented as,

$$\hat{\mathcal{A}}_k = \arg \min_{A_k^{(i)},\, i \in \mathbb{M}_P} \left| r_k r_{k+1}^* - A_k^{(i)} \right|^2. \tag{12}$$

Once $\hat{\mathcal{A}}_k$ is obtained, we can compute $\hat{\mathcal{H}}_k$ in a DD fashion as described in (6),

$$\hat{\mathcal{H}}_k = \frac{r_k}{\hat{\mathcal{A}}_k}. \tag{13}$$

Therefore, the proposed technique can be implemented by replacing the pilot symbols with data symbols that have CM, and using MASK to modulate the adjacent subcarriers, $A_{k+1} \in \mathbb{R}^+$. Finally, $\hat{H}_k$ can be obtained from $\hat{\mathcal{H}}_k$ using any technique that is originally used in conjunction with pilot-based systems [12], [34], [35]. The proposed channel estimator transmitter and receiver block diagrams are depicted in Figs. 2 and 3, respectively. At the transmitter, the information bits are applied to a channel encoder, which is an optional function, then the encoded bits are split into three parallel streams each of which is modulated using the corresponding modulation scheme. The three types of symbols are combined to form one block, and the rest of the process is similar to conventional OFDM transmission.

As compared to other practical OFDM-based systems such as LTE-A, it can be noted that the proposed transmitter is generally similar to such systems except that the pilot subcarriers are replaced with MPSK information symbols and the adjacent subcarriers are modulated using MASK as shown in Fig. 1b. It is worth noting that pilot symbols in LTE-A are originally modulated using QPSK, however, they do not bear information. Moreover, the symbols adjacent to the pilots can be modulated using QPSK, 16 or 64 QAM, which does not allow extracting the channel information directly from such modulation schemes. Therefore, MASK is used to estimate the channel phase directly from the received symbols, and hence allow coherent detection of the QPSK symbols in the pilots locations.

The MASK modulated symbols A_{k+1} can be designed such that the average power is normalized to unity, $\mathcal{P}_s = \frac{1}{M_A}\sum_{i=0}^{M_A-1}\left(A_{k+1}^{(i)}\right)^2 = 1$. Assuming equally spaced amplitudes, the amplitude spacing $\delta \triangleq A_{k+1}^{(i+1)} - A_{k+1}^{(i)}$ [15] can be written as

$$A_{k+1}^{(i)} = (i+1) \times \delta,\ i \in \{0, 1, \ldots, M_A - 1\} \tag{14}$$

where,

$$\delta = \sqrt{\frac{6}{(2M_A+1)(M_A+1)}}. \tag{15}$$

For all other subcarriers other than the pilots' and their adjacent subcarriers, the modulation type and order can be chosen arbitrarily. Moreover, although the OSBCE is applied to LTE-A, it can be applied to other OFDM-based systems where the frequency spacing Δ_F and time spacing Δ_T can be changed based on the corresponding system specifications.

As it can be noted from the system description, the computational complexity of the OSBCE is equivalent to LSE using pilots. Particularly, when considering that $\hat{\mathcal{A}}_k = \hat{A}_k$, which

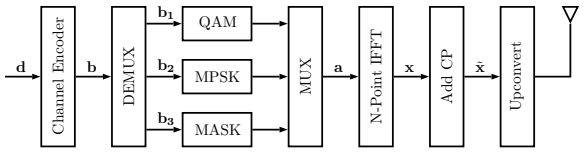

Fig. 2. Block diagram of the proposed transmitter.

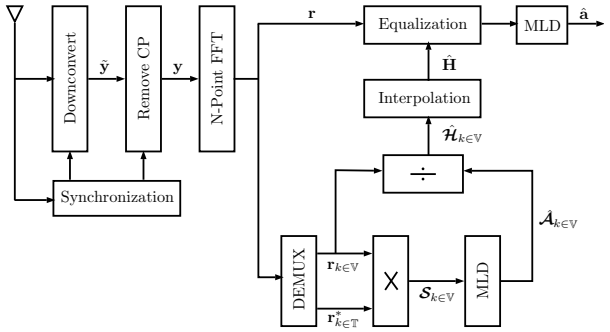

Fig. 3. Block diagram of the proposed receiver.

is mainly the case because for most interpolation techniques $\hat{H}_k \approx \tilde{\mathcal{H}}_k$. In the case that a new detection is applied after the estimation of $\hat{\mathbf{H}}$, then the only additional complexity, as compared to pilot systems, is N_P complex multiplications and MLD detections applied to the N_P MPSK symbols. Therefore, the proposed OSBCE complexity is generally low, and it is equivalent to pilot-based channel estimators.

IV. Symbol Error Rate (SER) Analysis

Because the OSBCE operates as a DD estimator, its MSE depends on the initial SER, $\Pr\left(\hat{\mathcal{A}}_k \neq A_k\right)$. Therefore, this section is dedicated to the derivation of the initial SER, then the MSE derivation is presented in the next section.

As it can be noted from (12), eliminating the fading channel effect using the product $r_k r_{k+1}^*$ is equivalent to conventional equalization of MPSK symbols, which is independent of the CFR magnitude $|H_k|$. However, the equalized samples can be also written as $r_k/r_{k+1} \triangleq \mathcal{S}_k$, where

$$\begin{aligned}\mathcal{S}_k &= \frac{H_k A_k + w_k}{H_{k+1}A_{k+1} + w_{k+1}} \\ &= \frac{A_k\,|H_k|\,e^{j(\theta_k - \hat{\vartheta}_{k+1})} + |w_k|\,e^{j\left(\arg(w_k) - \hat{\vartheta}_{k+1}\right)}}{|H_{k+1}A_{k+1} + w_{k+1}|} \\ &= \frac{1}{|r_{k+1}|}\left(|H_k|\,e^{j\psi_k}\;A_k + \acute{w}_k\right) \end{aligned} \tag{16}$$

where $\psi_k = \theta_k - \hat{\vartheta}_{k+1}$, $\acute{w}_k = |w_k|\,e^{j\left(\arg(w_k) - \hat{\vartheta}_{k+1}\right)}$ is a zero-mean complex Gaussian random variable whose variance is the same as that of w_k. Therefore, the equalized sample $\mathcal{S}_k$ in (16) has the form of MPSK symbol equalized using imperfect channel estimate. However, the conditional BER of BPSK and QPSK modulations in fading channels with imperfect knowledge of the CFR parameters can be expressed as [36, 10.14a],

$$P_{B,k|}\left[\psi_k, \alpha_k\right] = Q\left(\frac{\alpha_k}{\sigma_w}\cos(\psi_k)\right) \tag{17}$$

and

$$\begin{aligned}P_{B,k|}\left[\psi_k, \alpha_k\right] = &\frac{1}{2}Q\left(\frac{\alpha_k}{\sqrt{2}\sigma_w}\left[\cos(\psi_k) - \sin(\psi_k)\right]\right) \\ &+ \frac{1}{2}Q\left(\frac{\alpha_k}{\sqrt{2}\sigma_w}\left[\cos(\psi_k) + \sin(\psi_k)\right]\right)\end{aligned} \tag{18}$$

where $\alpha_k = |H_k|$ is the fading envelope of the kth subcarrier, and $Q(x) \triangleq 1/\sqrt{2\pi}\int_x^\infty e^{-t^2/2}dt$. Consequently, the conditioning on α_k and ψ_k can be eliminated by averaging (17) and (18) over the joint probability density function (PDF) $P(\psi_k, \alpha_k)$. To simplify the solution, we initially assume that the MASK symbol A_{k+1} is fixed, and hence, the conditional BER can be computed as,

$$P_{B,k} = \int_0^\infty \int_{-\pi}^{\pi} P_{B,k|}\left[\psi_k, \alpha_k\right]\; P(\alpha_k, \psi_k)\; d\psi_k\; d\alpha_k. \tag{19}$$

Although A_{k+1} is not written explicitly in (17), (18) and the joint PDF $P(\alpha_k, \psi_k)$, it is actually included in the conditioning on ψ_k,because $\psi_k = \theta_k - \arg\left\{H_{k+1}A_{k+1} + w_{k+1}\right\}$.

The joint PDF $P(\alpha_k, \psi_k)$ can be obtained by following the approach reported in [27], where r_k and r_{k+1} are expressed as,

$$r_k = H_k A_k + w_k,\;\; H_k \triangleq x_1 + jx_2 = \alpha_k e^{j\theta_k} \tag{20}$$

$$r_{k+1} = H_{k+1}A_{k+1} + w_{k+1} \triangleq x_3 + jx_4 = \beta_k e^{j\hat{\vartheta}_k}. \tag{21}$$

The random variables $\{x_1,\, x_2,\, x_3,\, x_4\}$ are all zero-mean Gaussian random variables, where x_1 and x_2 are independent, x_3 and x_4 are independent as well, thus $E\left\{x_1 x_2\right\} = E\left\{x_3 x_4\right\} = 0$. Therefore, the joint PDF $P(x_1,\, x_2,\, x_3,\, x_4)$ can be described by (22) (at the top of the next page),

where σ_1, σ_2, μ_1, and μ_2 are given by [37],

$$\sigma_1^2 \triangleq E\left\{x_1^2\right\} = E\left\{x_2^2\right\} = \frac{1}{2}E\left\{|H_k|^2\right\} = \sigma_H^2 \tag{23}$$

$$\begin{aligned}\sigma_2^2 \;&\triangleq\; E\left\{x_3^2\right\} = E\left\{x_4^2\right\} = \frac{1}{2}E\left\{|r_{k+1}|^2\right\} \\ &=\; \frac{1}{2}E\left\{|H_{k+1}A_{k+1} + w_{k+1}|^2\right\} \\ &=\; \sigma_H^2\,|A_{k+1}|^2 + \sigma_w^2\end{aligned} \tag{24}$$

$$\begin{aligned}\mu_1 + j\,\mu_2 \triangleq\; &\frac{1}{2}\left[E\left\{(r_{k+1})\,H_k^*\right\}\right] \\ &= A_{k+1}\sum_{n=0}^{L_{\rm h}} \sigma_{h_n}^2 \cos\left(2\pi\frac{n}{N}\right) \\ &\quad + jA_{k+1}\sum_{n=0}^{L_{\rm h}} \sigma_{h_n}^2 \sin\left(2\pi\frac{n}{N}\right).\end{aligned} \tag{25}$$

By making the transformation from rectangular $(x_1,\, x_2,\, x_3,\, x_4)$ to polar coordinates $(\alpha_k, \beta_k, \theta_k, \hat{\vartheta}_k)$, and applying the following change of variables

$$\begin{aligned}x_1 = \alpha_k\cos(\theta_k),\; x_2 = \alpha_k\sin(\theta_k) \\ x_3 = \beta_k\cos(\hat{\vartheta}_k),\; x_4 = \beta_k\sin(\hat{\vartheta}_k),\; \psi_k = \theta_k - \hat{\vartheta}_k\end{aligned} \tag{26}$$

$$P(x_1,x_2,x_3,x_4)=\frac{1}{4\pi^2(\sigma_1^2\sigma_2^2-\mu_1^2-\mu_2^2)}\exp\left[-\frac{\sigma_2^2(x_1^2+x_2^2)+\sigma_1^2(x_3^2+x_4^2)-2\mu_1(x_1x_3+x_2x_4)-2\mu_2(x_1x_4-x_2x_3)}{2(\sigma_1^2\sigma_2^2-\mu_1^2-\mu_2^2)}\right]. \tag{22}$$

the following joint PDF can be obtained,

$$P(\alpha_k,\psi_k)=\int_0^\infty \frac{\alpha_k\beta_k}{2\pi\sigma_1^2\sigma_2^2(1-\rho^2)}\exp\left\{-\frac{1}{2(1-\rho^2)}\times\left[\frac{\alpha_k^2}{\sigma_1^2}+\frac{\beta_k^2}{\sigma_2^2}-2\frac{\alpha_k\beta_k}{\sigma_1\sigma_2}\left(\rho_1\cos(\psi_k)-\rho_2\sin(\psi_k)\right)\right]\right\}d\beta_k \tag{27}$$

where the correlation coefficients are defined by

$$\rho_1\triangleq\frac{\mu_1}{\sigma_1\sigma_2},\ \rho_2\triangleq\frac{\mu_2}{\sigma_1\sigma_2},\ \rho\triangleq\sqrt{\rho_1^2+\rho_2^2}. \tag{28}$$

Substituting (17), (18) and (27) into (19), and using the integral identity established in [27, Appendix B], we get the closed-form BER conditioned on A_{k+1} for BPSK as,

$$P_{B,k}=\frac{1}{2}\left[1-\frac{\rho_1}{\sqrt{1+\frac{1}{\mathrm{SNR}}-\rho_2^2}}\right] \tag{29}$$

and for QPSK

$$P_{B,k}=\frac{1}{2}\left[1-\frac{1}{2}\frac{\rho_1+\rho_2}{\sqrt{2+\frac{1}{\mathrm{SNR}}-(\rho_1-\rho_2)^2}}+\frac{\rho_1-\rho_2}{\sqrt{2+\frac{1}{\mathrm{SNR}}-(\rho_1+\rho_2)^2}}\right]. \tag{30}$$

It is worth noting that the SNR per bit γ_b is defined as

$$\begin{aligned}\gamma_b&\triangleq\frac{E\left\{|H_kA_k|^2\right\}}{\log_2(M_P)\ E\left\{|w_k|^2\right\}}\\&=\frac{\mathcal{P}_s}{\sigma_w^2}\frac{\sigma_1^2}{\log_2(M_P)}\\&=\frac{\mathrm{SNR}}{\log_2(M_P)}.\end{aligned} \tag{31}$$

Given that the average symbol power $\mathcal{P}_s=E\left\{|A_k|^2\right\}=1$, the SNR per bit γ_b can be written as

$$\gamma_b\triangleq\frac{\sigma_1^2}{\log_2(M_P)\ \sigma_w^2}. \tag{32}$$

The parameters σ_2, μ_1 and μ_2 are functions of the MASK symbol A_{k+1}, and hence the average unconditioned BER can be obtained by averaging (29) and (30) over all possible values of A_{k+1}. Since $A_{k+1}^{(i)}$ are equally probable, the average $\bar{P}_{B,k}$ becomes,

$$\bar{P}_{B,k}=\frac{1}{M_A}\sum_{i=0}^{M_A-1}\left(P_{B,k}|A_{k+1}^{(i)}\right). \tag{33}$$

Moreover, assuming Gray coding, the SER for QPSK is given by [38, 8.7],

$$\bar{P}_{S,k}=2\bar{P}_{B,k}. \tag{34}$$

V. Mean Squared Error (MSE) Analysis

The MSE of the initial CFR estimate $\hat{\mathcal{H}}_k$ is given by

$$\mathrm{MSE}(\hat{\mathcal{H}}_k)=E\left\{\left|\hat{\mathcal{H}}_k-H_k\right|^2\right\} \tag{35}$$

where

$$\hat{\mathcal{H}}_k=\frac{r_k}{\hat{\mathcal{A}}_k}=H_k\frac{A_k}{\hat{\mathcal{A}}_k}+\frac{w_k}{\hat{\mathcal{A}}_k}. \tag{36}$$

To simplify the notations, $\mathrm{MSE}(\hat{\mathcal{H}}_k)$ is written as MSE, unless it is necessary to write the full expression. Substituting (36) into (35) gives

$$\mathrm{MSE}=E\left\{\left|H_k\frac{A_k}{\hat{\mathcal{A}}_k}+\frac{w_k}{\hat{\mathcal{A}}_k}-H_k\right|^2\right\}. \tag{37}$$

Because $\hat{\mathcal{A}}_k$ may take one of two states, the law of total probability can be used to decompose the MSE as the sum of two conditional scenarios,

$$\mathrm{MSE}=(\mathrm{MSE}|D_C)\Pr(D_C)+(\mathrm{MSE}|D_I)\Pr(D_I) \tag{38}$$

where the events of correct and incorrect decisions are denoted by D_C and D_I, respectively, and $\Pr(D_I)=\Pr\left(\hat{\mathcal{A}}_k\neq A_k\right)=P_{S,k}$ and $\Pr(D_C)=\Pr\left(\hat{\mathcal{A}}_k=A_k\right)=P_{C,k}=1-P_{S,k}$. To simplify the presentation, the two conditional cases are presented into the following two subsections.

A. $\mathrm{MSE}\left(\hat{\mathcal{H}}_k|D_C\right)$

For the case of $\hat{\mathcal{A}}_k=A_k$, the conditional initial channel estimate can be expressed as,

$$\hat{\mathcal{H}}_k|D_C=H_k|D_C+\frac{w_{k|D_C}}{A_k}. \tag{39}$$

Therefore, the conditional MSE can be computed as

$$\mathrm{MSE}|D_C=E\left\{\left|\left(\hat{\mathcal{H}}_k\,|\,D_C\right)-\left(H_k\,|\,D_C\right)\right|^2\right\}. \tag{40}$$

It is worth noting that the conditioning on the right hand side of (40) is necessary due to the correlation between the estimated MPSK symbol $\hat{\mathcal{A}}_k$, H_k and the AWGN samples w_k, which is due to the fact that the event $\hat{\mathcal{A}}_k=A_k$ is generally realized at high H_k values and low w_k values. Therefore, substituting (39) in (40) gives

$$\mathrm{MSE}|D_C=E\left\{\left|\frac{w_k\ |\ D_C}{A_k}\right|^2\right\}. \tag{41}$$

The result in (41) is expected because the process is generally similar to the conventional LSE. However, $w_k|D_C$ is a sampled version of w_k because the conditioning process on D_C eliminates most of the high power noise samples, and hence, $E\left\{|w_k|D_C|^2\right\}\neq E\left\{|w_k|^2\right\}$. Fig. 4 shows the

This article has been accepted for publication in a future issue of this journal, but has not been fully edited. Content may change prior to final publication. Citation information: DOI 10.1109/TCOMM.2017.2740925, IEEE Transactions on Communications

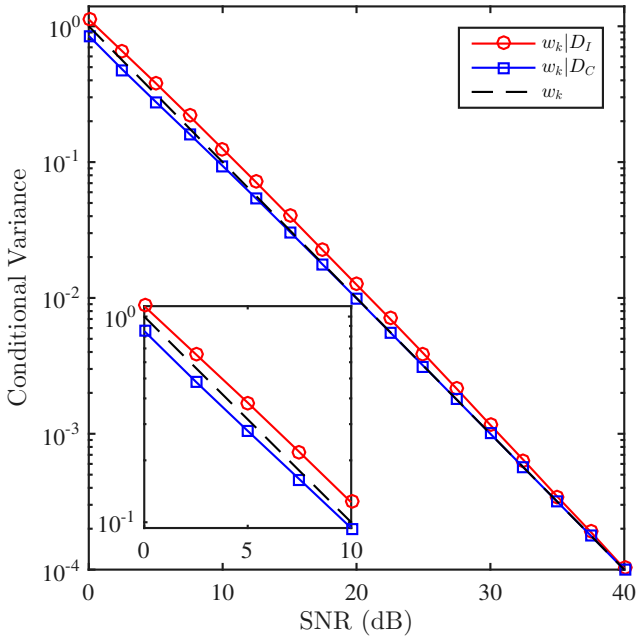

Fig. 4. Conditional AWGN variance in the case of correct and incorrect decisions compared to the unconditional variance of AWGN for the TUx channel, $M_P = 4$, $M_A = 4$.

AWGN variance conditioned on D_C versus SNR as compared to the unconditional AWGN. The channel is modeled as a typical urban (TUx) multipath channel [40], which is described in Section VII. It can be noticed from the figure that $E\left\{|w_k \nmid D_C|^2\right\} < E\left\{|w_k|^2\right\}$ at low SNRs, and they converge for SNR $\gtrsim 10$ dB. Such behavior is due to the fact that the effect of noise sampling disappears at high SNRs because the channel fading is the dominant parameter that determines the outcome of the detection process. Therefore, it can be assumed without sacrificing the accuracy that,

$$\begin{aligned}\mathrm{MSE}|D_C &= E\left\{\left|\frac{w_k \mid D_C}{A_k}\right|^2\right\} \\ &\approx E\left\{\left|\frac{w_k}{A_k}\right|^2\right\} \\ &= \frac{1}{\mathrm{SNR}}. \end{aligned} \tag{42}$$

B. MSE $\left(\hat{\mathcal{H}}_k|D_I\right)$

For the case where $\hat{\mathcal{A}}_k \neq A_k$, the MSE can be obtained by substituting

$$\hat{\mathcal{H}}_k|D_I = (H_k|D_I)\frac{A_k}{\hat{\mathcal{A}}_k} + \frac{w_k|D_I}{\hat{\mathcal{A}}_k} \tag{43}$$

in (35), which gives

$$\mathrm{MSE}|D_I = E\left\{\left|(H_k \mid D_I)\frac{A_k}{\hat{\mathcal{A}}_k} + \frac{w_k|D_I}{\hat{\mathcal{A}}_k} - (H_k \mid D_I)\right|^2\right\}. \tag{44}$$

By assuming that all transmitted symbols are equiprobable [41], we assume, without loss of generality, that the MPSK symbol $A_k^{(0)} = e^{j\pi/M_P}$ is transmitted, and hence, $\hat{\mathcal{A}}_k = e^{j\pi(2i+1)/M_P}$, $i \in \{1, 2, \ldots, M_P - 1\}$. By defining $\varphi_k \triangleq \arg\left\{A_k^{(0)}/\hat{\mathcal{A}}_k\right\}$, then (44), after some straightforward manipulations becomes

$$\begin{aligned}\mathrm{MSE}|D_I = E\left\{\left|\frac{w_k \mid D_I}{\hat{\mathcal{A}}_k}\right|^2\right\} \\ + 2E\left\{|H_k|^2 \nmid D_I\right\}\left(1 - E\left\{\cos(\varphi_k)|D_I\right\}\right). \end{aligned} \tag{45}$$

Contrary to the D_C case, the conditional noise variance $E\left\{|w_k \nmid D_I|^2\right\}$ is slightly higher than the unconditional noise variance $E\left\{|w_k|^2\right\}$ at low SNRs, then the difference disappears for SNR $\gtrsim 40$ dB as shown in Fig. 4. Therefore, $E\left\{|w_k \nmid D_I|^2\right\} \approx E\left\{|w_k|^2\right\} = \frac{1}{\mathrm{SNR}}$. Similar to the AWGN case, the incorrect decision event D_I and the CFR H_k are correlated as well. Since most error events occur in deep fading conditions, then $E\left\{\alpha_k^2|D_I\right\} \ll E\left\{\alpha_k^2\right\}$. Therefore, to evaluate MSE $|D_I$ in (45), the terms $E\left\{\cos(\varphi_k)|D_I\right\}$ and $E\left\{\alpha_k^2|D_I\right\}$ should be evaluated first.

- $E\left\{\cos(\varphi_k)|D_I\right\}$:

Because φ_k is a discrete random variable, the conditional expectation can be expressed as

$$E\left\{\cos(\varphi_k)|D_I\right\} = \sum_{\varphi_k} \Pr\left(\varphi_k|\, D_I\right)\cos(\varphi_k) \tag{46}$$

where $\varphi_k = \frac{-2\pi i}{M_P}$, $i \in \{1, 2, \ldots, M_P - 1\}$. For example, $\Pr\left(\varphi_k = \frac{-2\pi}{M_P}\right) = \Pr\left(\hat{\mathcal{A}}_k = A_k^{(1)}\right)$. Recalling Bayes' theorem with mixed distributions, the conditional probability $\Pr\left(\varphi_k|D_I\right)$ can be evaluated as

$$\Pr\left(\varphi_k|\, D_I\right) = \frac{1}{\Pr\left(D_I\right)}\Pr\left(D_I|\varphi_k\right)\Pr\left(\varphi_k\right). \tag{47}$$

By noting the definition of φ_k and the fact that the transmitted symbol is $A_k^{(0)}$, then $\Pr\left(D_I|\varphi_k\right) = 1$, and hence,

$$\Pr\left(\varphi_k|\, D_I\right) = \frac{1}{P_{S,k}}\Pr\left(\varphi_k\right) \tag{48}$$

where

$$\Pr\left(\varphi_k\right) = \int_{\frac{2\pi i}{M_P}}^{\frac{2\pi(i+1)}{M_P}} P(\Theta_k)d\Theta_k,\ i \in \{1, 2, ..., M_P - 1\} \tag{49}$$

and

$$\Theta_k = \arg\left\{r_{k+1}^* r_k\right\}. \tag{50}$$

However, at high SNRs $\Theta_k \approx \arg\{A_k\} + \psi_k$, and since it is assumed that $A_k = A_k^{(0)} = e^{j\pi/M_P}$, then $\arg\{A_k\} = \pi/M_P$. Therefore (49) can be expressed as

$$\Pr\left(\varphi_k\right) = \int_{\frac{\pi(2i-1)}{M_P}}^{\frac{\pi(2i+1)}{M_P}} P(\psi_k)d\psi_k,\ i \in \{1, 2, ..., M_P - 1\} \tag{51}$$

where $P(\psi_k)$, which can be obtained from (27),

$$\begin{aligned} P(\psi_k) &= \int_0^\infty P(\alpha_k, \psi_k)\ d\beta_k\ d\alpha_k \\ &= \frac{1-\rho^2}{2\pi\left[1-\zeta_k^2\right]^{\frac{3}{2}}}\zeta_k\ \arctan\left(\frac{\zeta_k}{\sqrt{1-\zeta_k^2}}\right) \\ &\quad + 2\sqrt{1-\zeta_k^2} + \pi\zeta_k \end{aligned} \tag{52}$$

and $\zeta_k = \rho_1\cos(\psi_k) + \rho_2\sin(\psi_k)$. Finally, $\Pr(\varphi_k|\, D_I)$ is given by

$$\Pr(\varphi_k|\, D_I) = \frac{1}{P_{S,k}}\int_{\frac{\pi(2i-1)}{M_P}}^{\frac{\pi(2i+1)}{M_P}} P(\psi_k)d\psi_k. \tag{53}$$

To the best of our knowledge, the integral in (53) has no closed form expression, and hence, it will be evaluated numerically.

- $E\left\{\alpha_k^2|D_I\right\}$:

The conditional variance of H_k can be computed as

$$E\left\{\alpha_k^2|D_I\right\} = \int_0^\infty \alpha_k^2 P(\alpha_k|D_I)d\alpha_k \tag{54}$$

Using Bayes' rule with mixed distributions, the conditional PDF $P(\alpha_k|D_I)$ can be evaluated as

$$\begin{aligned} P(\alpha_k|D_I) &= \frac{\Pr(D_I|\alpha_k)P(\alpha_k)}{\Pr(D_I)} \\ &= \frac{\left(P_{S,k}|\alpha_k\right)P(\alpha_k)}{P_{S,k}}. \end{aligned} \tag{55}$$

By noting that the $P_{S,k} = P_{B,k}$ for the BPSK and using (34) for QPSK, then $P(\alpha_k|D_I)$ which is given by (55) can be simplified to

$$P(\alpha_k|D_I) = \frac{\log_2(M_P)}{P_{S,k}}\left(P_{B,k}|\alpha_k\right)P(\alpha_k). \tag{56}$$

Using the joint PDF $P(\alpha_k, \psi_k)$ in (27), and the conditional BER for BPSK (17) or QPSK (18), then $E(\alpha_k^2|D_I)$ can be computed as as depicted in (57) (at the top of the next page).

Finally, the $\mathrm{MSE}(\hat{\mathcal{H}}_k)$ can be written as

$$\begin{aligned} \mathrm{MSE}(\hat{\mathcal{H}}_k) &= (\mathrm{MSE}\,|D_C)P_{C,k} + (\mathrm{MSE}\,|D_I)P_{S,k} \\ &= \frac{1}{\mathrm{SNR}} + 2P_{S,k}E\left\{\alpha_k^2|D_I\right\} \\ &\quad \times\left(1 - E\left\{\cos(\varphi_k)|D_I\right\}\right). \end{aligned} \tag{58}$$

By noting that most of the terms in (58) are dependent on A_{k+1}, then the unconditional MSE can be expressed as

$$\overline{\mathrm{MSE}}(\hat{\mathcal{H}}_k) = \frac{1}{M_A}\sum_{i=0}^{M_A-1}\left(\mathrm{MSE}(\hat{\mathcal{H}}_k)\mid A_{k+1}^{(i)}\right). \tag{59}$$

Moreover, by noting that $E\left\{\alpha_k^2|D_I\right\} \le 2\sigma_H^2$, and noting that $-1 \le \cos(\varphi_k) \le 1$, and hence an upper and lower bounds can be expressed as

$$\frac{1}{\mathrm{SNR}} \le \mathrm{MSE} \le \frac{1}{\mathrm{SNR}} + 8\sigma_H^2\bar{P}_{S,k}. \tag{60}$$

VI. Spectral Efficiency

In this section, the spectral efficiency of the OSBCE is evaluated in terms of the throughput, which is defined as the average number of information bits per subcarrier. In the most general case, each subcarrier in an OFDM grid can be modulated using a certain modulation scheme with a particular modulation order. Therefore, the average number of information bits over one OFDM grid can be expressed as,

$$\eta = \frac{1}{N_T \times N_F}\sum_{\ell=0}^{N_T-1}\sum_{k=0}^{N_F-1}\log_2\left[M(\ell,k)\right]. \tag{61}$$

where $M(\ell,k)$ is the modulation order at a given location (ℓ,k), N_T and N_F are the time and frequency dimensions of the OFDM grid, respectively. Fig. 1a shows an example where $N_T = 14$ and $N_F = 12$.

In practical systems, the value of $M(\ell,k)$ is dynamically selected based on the system QoS requirements, the system resources, modulation order constrains, and the channel state information (CSI) [39]. Without loss of generality, consider the case where the values of $M(\ell,k)$ can be selected dynamically with the aim of maximizing the throughput of a particular system under BER, and modulation type/order constraints. Therefore, the problem can be formulated as

$$\max_{M(\ell,k)\in\mathbb{M}}\ \frac{1}{N_T \times N_F}\sum_{\ell=0}^{N_T-1}\sum_{k=0}^{N_F-1}\log_2\left[M(\ell,k)\right] \tag{62a}$$

Subject to:

$$\bar{P}_B \le P_{th} \tag{62b}$$

where $\mathbb{M}$ is the set of all possible modulation orders, and (62b) is used to guarantee that the average BER $\bar{P}_B$ is less than a prescribed threshold P_{th},

$$\bar{P}_B = \frac{\sum_{\ell=0}^{N_T-1}\sum_{k=0}^{N_F-1}\log_2\left(M(\ell,k)\right)P_B\left(\gamma_{\ell,k}\,|_{M,T}\right)}{\sum_{\ell=0}^{N_T-1}\sum_{k=0}^{N_F-1}\log_2\left(M(\ell,k)\right)} \le P_{th} \tag{63}$$

where $P_B\left(\gamma_{\ell,k}\,|_{M,T}\right)$ is the instantaneous BER for a given value of M and modulation type T, and the instantaneous SNR is denoted by $\gamma_{\ell,k} = |A_{k,\ell}|^2 \cdot |H_{k,\ell}|^2 / \left(2\sigma_w^2\right)$. Assuming that the possible modulation types are QAM, MPSK and MASK, then $P_B\left(\gamma_{\ell,k}\,|_{M_Q,\,\mathrm{QAM}}\right)$ and $P_B\left(\gamma_{\ell,k}\,|_{M_P,\,\mathrm{MPSK}}\right)$ are given in [37], while $P_B\left(\gamma_{\ell,k}\,|_{M_A,\,\mathrm{MASK}}\right)$ under the Gray coding assumption is given by

$$\begin{aligned} P_B\left(\gamma_{\ell,k}\,|_{M_A,\,\mathrm{MASK}}\right) &= \frac{2\,(M_A-1)}{M_A\log_2(M_A)} \\ &\quad \times Q\left(\sqrt{\frac{3\,\gamma_{k,\ell}}{4M_A^2+6M_A+2}}\right). \end{aligned} \tag{64}$$

It is worth noting that P_B for the considered modulation schemes is computed while assuming perfect knowledge of the instantaneous SNRs $\gamma_{\ell,k}$. Therefore, the obtained throughput in (62) can be considered an upper bound because channel estimation errors may degrade the SNRs, and hence, reduce the throughput for all the considered techniques.

For a fair comparison between various systems, the power efficiency should be also taken into consideration. Therefore,

$$E\left\{\alpha_k^2|D_I\right\} = \frac{\log_2(M_P)}{P_{S,k}} \int_0^{\infty}\int_0^{\infty}\int_{-\pi}^{\pi} \alpha_k^2 \left(P_{B,k}|\psi_k,\alpha_k\right)\ P(\alpha_k,\beta_k,\psi_k)d\psi_k\ d\beta_k\ d\alpha_k \tag{57}$$

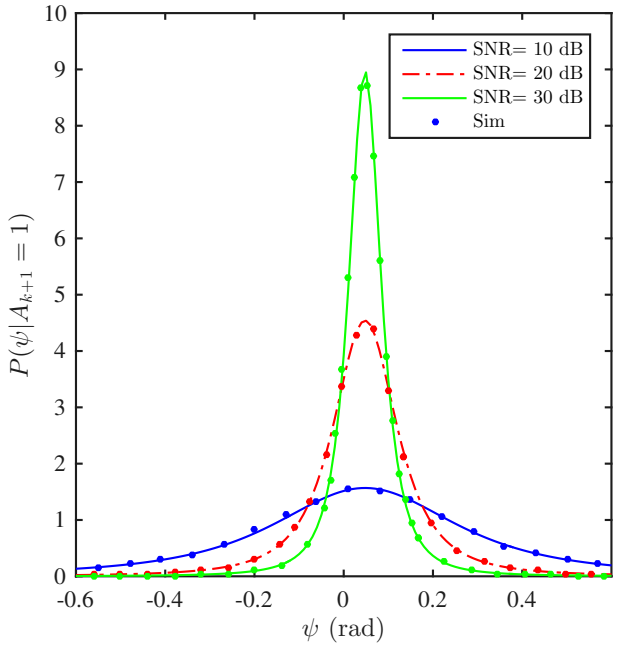

Fig. 5. $P(\psi)$ for different values of SNR over the TUx channel where $A_{k+1}=1$, $M_P=4$, and $M_A=4$.

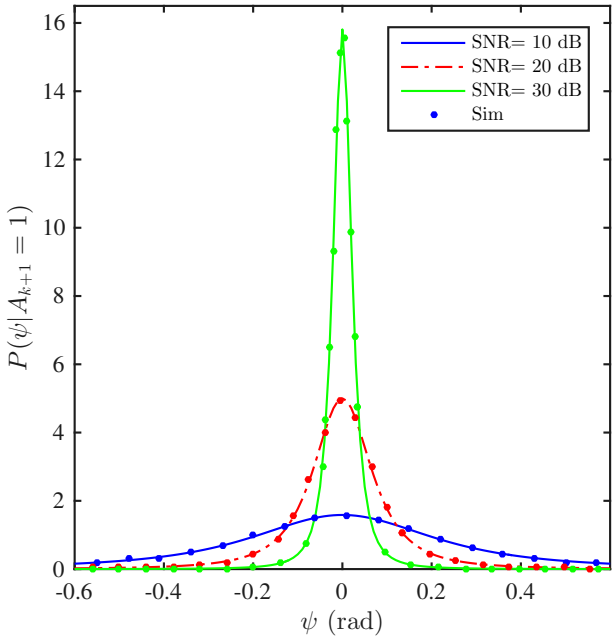

Fig. 6. $P(\psi)$ for different values of SNR over a flat fading channel where $A_{k+1}=1$, $M_P=4$, and $M_A=4$.

the power per information subcarrier in the blind system $P_{SC,blind}$ should be equal to that in the pilot-based system $P_{SC,pilot}$. Consequently,

$$P_{SC,blind} = \frac{N_F \times N_T}{N_F \times N_T - N_{P,\mathrm{RB}}} P_{SC,pilot} \tag{65}$$

where $N_{P,\mathrm{RB}}$ is the number of pilot subcarriers per OFDM grid. However, since the MASK symbols in the OSBCE are the most sensitive symbols to noise, the additional power is allocated to them. Consequently, the power of each subcarrier with MASK modulation will be assigned an additional 3 dB gain.

VII. Numerical Results

The performance of the proposed OSBCE is evaluated over quasi-static flat and frequency-selective multipath fading channels, where the channel remains fixed over one transmission frame that consists of 7 OFDM symbols, but may vary randomly over consecutive frames. The proposed estimator is compared to pilot-based OFDM systems with the LTE transmission grid shown in Fig. 1a. The performance of the proposed estimator is evaluated in terms of SER and MSE.

The OFDM system considered follows the LTE downlink physical layer specifications [5] where the sampling frequency is 3.836 MHz, $N = 256$ subcarriers, $N_{\mathrm{CP}} = 18$ samples, subcarrier spacing is 15 kHz, total OFDM symbol period is 71.3 μsec, and CP period is 4.69 μsec. Two channel models are used, the flat fading and the TUx multipath fading model [40], which consists of 9 taps with normalized delays of [0, 1, ..., 8] samples, and the average taps' gains $2\sigma_{h_n}^2$, $n = [0, 1, \ldots, 8]$ are [0.269, 0.174, 0.289, 0.117, 0.023, 0.058, 0.036, 0.026, 0.008]. In each simulation run, 30×10^4 OFDM symbols are processed.

The PDF of the phase error ψ_k over the TUx and flat channels is given in Figs. 5 and 6, respectively, for SNR = 10, 20 and 30 dB given that $A_{k+1} = 1$. As expected, the figures show that the phase-error variance (σ_ψ^2) decreases as SNR increases, which implies that the channel estimates can be improved by increasing SNR. However for the TUx channel, Fig. 5 shows that the phase error is biased where $E\{\psi_k\} = \arg\{\varrho\} \neq 0$. Such bias is due to the fact that $\theta_k \neq \theta_{k+1}$ in frequency-selective channels, and hence, the multiplication process of $r_k r_{k+1}^*$ is equivalent to equalization with biased channel estimates, which causes SER error floors at high SNRs. Moreover, the figures show that σ_ψ^2 for the TUx channel is larger than that of the flat fading channel because the instantaneous difference between θ_k and θ_{k+1} is random, and hence contributes to σ_ψ^2. The figures also show the perfect match between the analytical and simulation results.

Fig. 7 shows $P(\psi_k)$ for different values of A_{k+1} at SNR = 20 dB. It can be noted that ψ_k is dependent on A_{k+1} where the variance decreases for high values of A_{k+1}. Such results imply that minimizing ψ_k can be obtained by maximizing A_{k+1}. However, since the possible values of A_{k+1} will affect

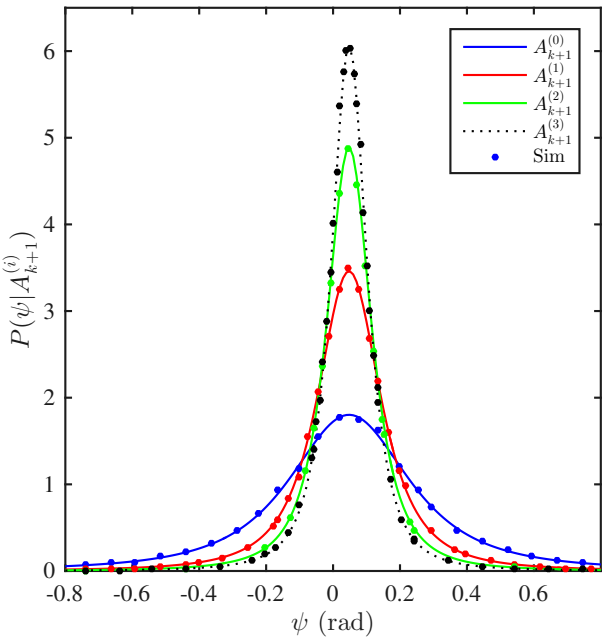

Fig. 7. $P(\psi)$ for different values of A_{k+1} over the TUx channel, SNR $= 20$ dB, $M_P = 4$, $M_A = 4$.

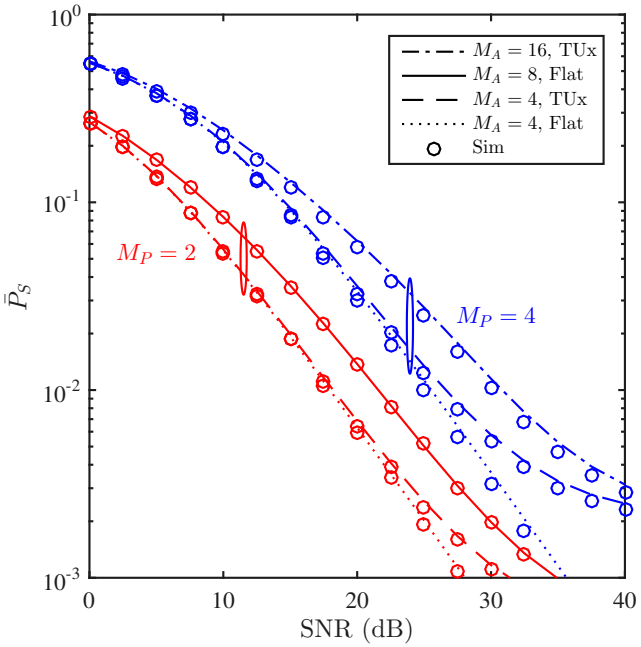

Fig. 8. Initial theoretical and simulated average SER $\Pr(\hat{\mathcal{A}}_k \neq A_k)\ \forall\, k \in \mathbb{V}$ over the TUx and flat channels.

$P_{S,k+1}$, then the optimal MASK amplitudes should be selected such that

$$\mathbf{a}_{k+1} = \arg \min_{\mathbf{a}_{k+1} \in \mathbb{R}^+} \sum_{i=0}^{N-1} P_{S,i} \tag{66}$$

where $\mathbf{a}_{k+1} = \left[A_{k+1}^{(0)}, A_{k+1}^{(1)}, ..., A_{k+1}^{(M_A-1)}\right]$ and $\frac{1}{M_A}\sum_{i=0}^{M_A-1}\left(A_{k+1}^{(i)}\right)^2 = 1$. However, solving such multi-objective optimization problem is computationally expensive, and hence we consider the equally spaced amplitudes for the purposes of this work.

The initial theoretical and simulated SER, $\Pr(\hat{\mathcal{A}}_k \neq A_k)\ \forall\, k \in \mathbb{V}$, of the MPSK symbols detected using (12) is depicted in Fig. 8. The results are presented for BPSK and QPSK using $M_A = 4$, 8 and 16, over the TUx and flat fading channels. The figure shows that the theoretical and simulation results match very well. However, a little difference can be observed for the QPSK case due to the approximation made in (18) [36], and the Gray coding assumption. Moreover, the impact of the channel frequency selectivity is observed only at high SNRs where an error floor starts to appear at SNR $\gtrsim 25$ dB.

Fig. 9 shows the impact of increasing the modulation order M_A, as well as the effect of the frequency selectivity of the channel on the initial SER, $\Pr(\hat{\mathcal{A}}_k \neq A_k)\ \forall k \in \mathbb{V}$. The figure shows that SER increases by increasing M_A which can be justified by noting that for $M_{A_1} < M_{A_2}$, $A_{k+1}^{(i)}|M_{A_1} > A_{k+1}^{(i)}|M_{A_2}\ \forall\ i \leq \min\{M_{A_1}, M_{A_2}\}$. In other words, increasing M_A will introduce more amplitudes with small values, which is equivalent to equalization using less reliable channel estimates. The figure also shows that at high SNRs, the impact of changing M_A vanishes for the TUx channel, because SER is determined by the frequency selectivity of the channel, which caused the bias of ψ_k. The flat channel kept at the same trends since SER will always be the dominant factor. Nevertheless, the initial SER remains sufficiently low to produce reliable channel estimates.

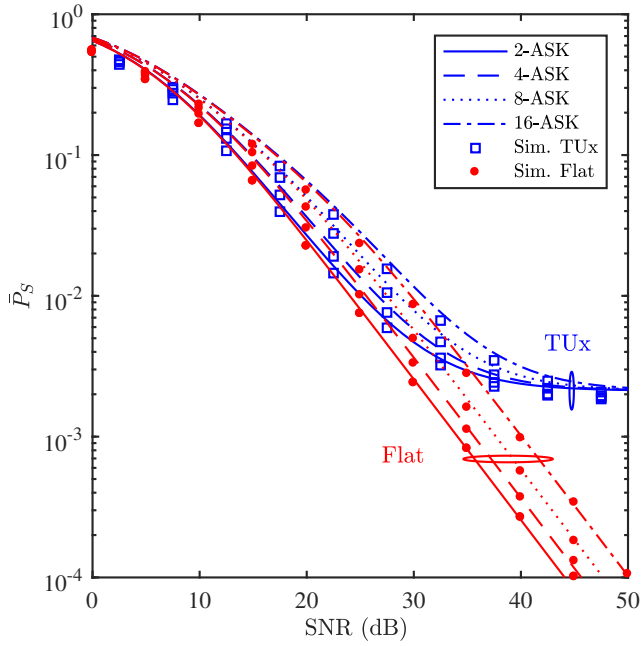

Fig. 9. Initial theoretical and simulated average SER $\Pr(\hat{\mathcal{A}}_k \neq A_k)\ \forall\, k \in \mathbb{V}$ over the TUx and flat channels for different values of M_A, and $M_P = 4$.

Fig. 10 shows the conditional variance of the CFR for $M_A = 4$, and for $M_P = 2$ and 4. As it can be noted from

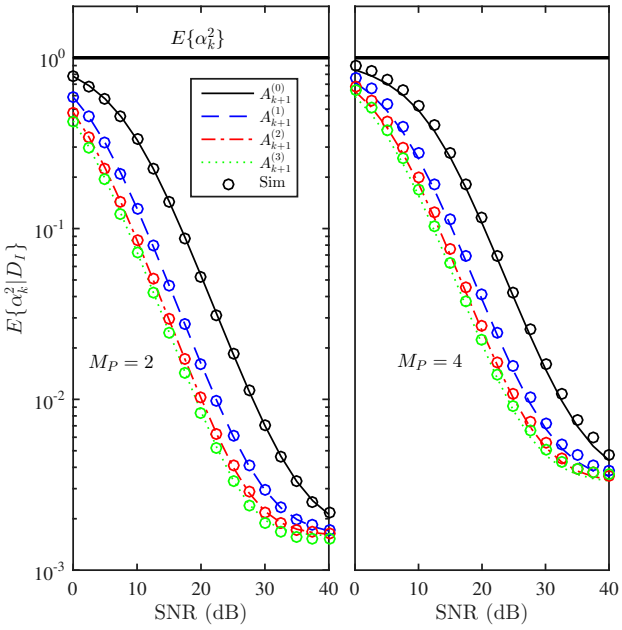

Fig. 10. Theoretical and simulated conditional CFR variance in the case of incorrect decisions as compared to the unconditional variance of CFR for the TUx channel, $M_P = 2$ and 4, $M_A = 4$.

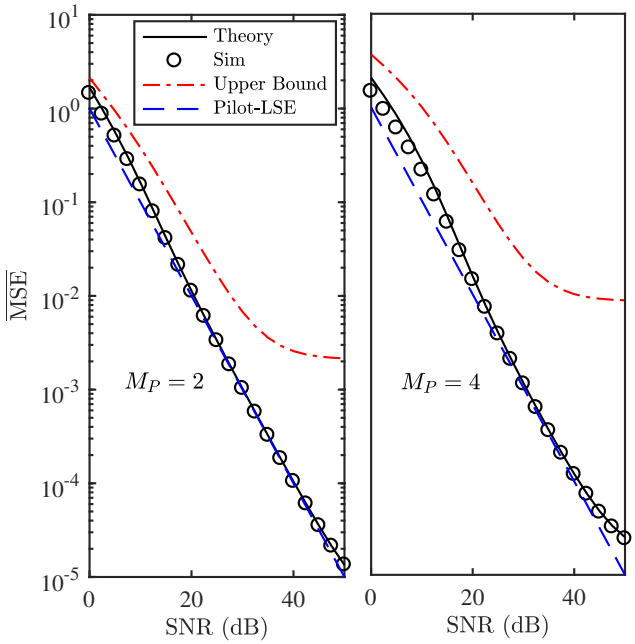

Fig. 11. MSE of the initial channel estimate $\hat{\mathcal{H}}_k$, $M_P = 2$ and 4, $M_A = 4$.

the figure, the difference between the conditional and unconditional variances is substantial, and it is inversely proportional to $A_{k+1}^{(i)}$, which is due to the fact that higher values of $A_{k+1}^{(i)}$ are more immune to fading, i.e., making an incorrect decision requires lower values of α_k. The results in the figure confirm the accuracy of the derived analytical expressions, however, the simulation results for the BPSK show better match because they are exact, while the QPSK results demonstrate some deviation due to the Gray coding approximation.

Fig. 11 presents the theoretical and simulated MSE versus SNR for BSK and QPSK respectively. As it can be noted from the figure, the analytical and simulation results match almost perfectly for SNR $\gtrsim$ 10 dB. However, the theoretical MSE of the QPSK slightly deviates from the simulation results at low SNRs due to the approximations made. Nevertheless, the results confirm the efficiency of the OSBCE because its MSE is comparable to pilot-based LSE for a wide range of SNRs, which is the lower bound for the MSE of the OSBCE. At very high SNRs, the MSE starts to diverge again from the lower bound because $P_{S,k}$ suffers from an error floor at such SNRs. However, the MSE at such high SNRs is much less than what is required to provide BERs close to those with perfect knowledge of CSI. Although the derived upper bound is loose, it is useful to get a general idea about the system MSE with minimum effort.

Fig. 12 presents the final SER, $\Pr(\hat{A}_k \neq A_k)$, of the OSBCE for two different groups of subcarriers. In one case $\bar{P}_{S,k}$ is computed for all subcarriers, and in the other case, $\bar{P}_{S,k}$ is computed for subcarriers with index $k \in \mathbb{U}$, i.e., all subcarriers except the MPSK data symbols at pilot locations and the adjacent MASK symbols. In all cases, the final channel

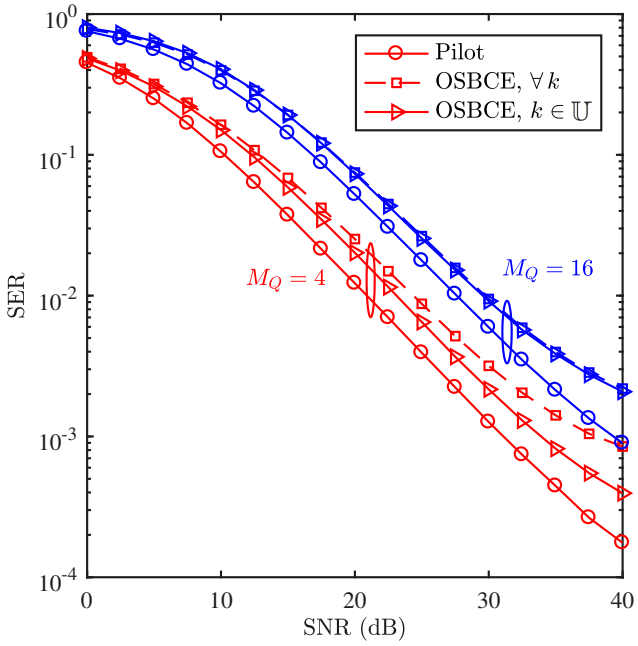

Fig. 12. Overall system SER, $\Pr(\hat{A}_k \neq A_k)$, using spline interpolation for different M_Q values, $M_P = 4$ and $M_A = 4$.

estimates $[\hat{H}_0, \hat{H}_1, \ldots, \hat{H}_{N-1}]$ are obtained using spline interpolation of the initial channel estimates $\hat{\mathcal{H}}_k$ $\forall k \in \mathbb{V}$. The SER results are compared to pilot-based systems where the initial channel estimates are obtained using LSE, and the final estimates are obtained using spline interpolation. For all OSBCE cases, the MASK modulation order $M_A = 4$, and the SNRs per information bit γ_b for all systems are identical.

This article has been accepted for publication in a future issue of this journal, but has not been fully edited. Content may change prior to final publication. Citation information: DOI 10.1109/TCOMM.2017.2740925, IEEE Transactions on Communications

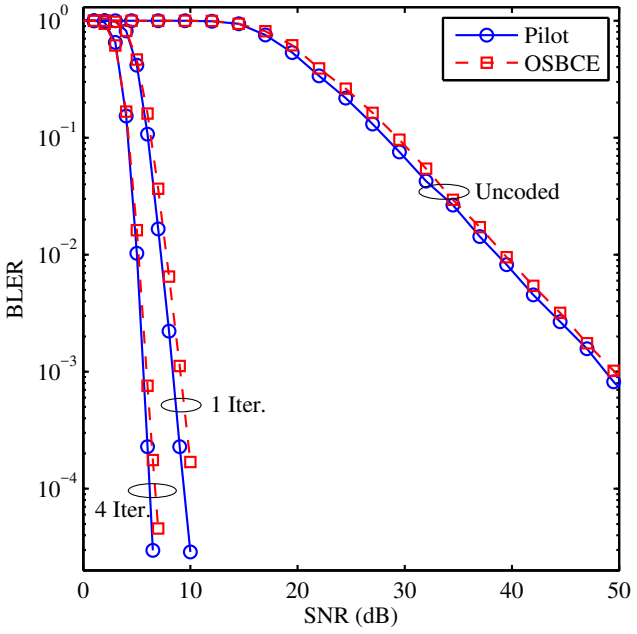

Fig. 13. Coded BLER for the OSBCE and pilot-based systems using one and four decoding iterations, $M_A = M_P = M_Q = 4$.

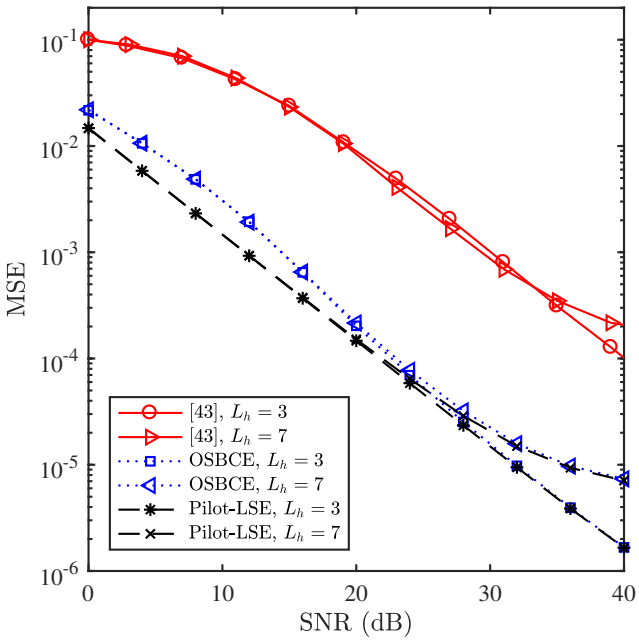

Fig. 14. MSE of the OSBCE and the subspace blind estimator [43], where $M_A = M_P = 4$.

As it can be noticed from the figure, the SER of the OSBCE where $k \in \mathbb{U}$ is about 3 dB worse than the pilot-based system at moderate SNR values for $M_Q = 4$ and 16. The difference increases at high SNRs due to the SER floors of the MASK modulation. For the SER of all subcarriers case, it can be noted that the SER when $M_Q = 4$ experiences an additional increase, which is due to the difference between the SER for MASK and QAM when $M_A = M_Q$. For the case of $M_A = 4$ and $M_Q = 16$, it can be noticed that the SER for $\forall k$ and $k \in \mathbb{U}$ is almost identical, which implies that the average joint SER of the 4-PSK and 4-ASK pairs is similar to the 16-QAM [42]. Therefore, under SER constraints, the OSBCE spectral efficiency could be less than the FB system.

Fig. 13 presents the block error rate (BLER) of the OSBCE and pilot-based systems using turbo coding [5]. The block length is 160 bits, and the channel interleaver is modeled as 512×512 random interleaver. As it can be noted from the figure, the BLER of the OSBCE is comparable to the pilot based system where the coding gain difference is less than 0.5 dB.

Fig. 14 presents the MSE of the OSBCE and the subspace estimator reported in [43]. Because the estimation process in [43] yields the channel impulse response, the channel impulse response using the OSBCE are obtained by interpolating the initial channel estimates, and then computing the IFFT. The results are obtained based on the system and channel models used in [43]. As it can be noted from the figure, the proposed OSBCE significantly outperforms the subspace estimator for the entire range of SNRs. Moreover, it is worth noting that the observation window in [43] is N/N_{CP} OFDM symbols, while it is only one OFDM symbol for the OSBCE.

The average throughput of the OSBCE, CM, pilot and

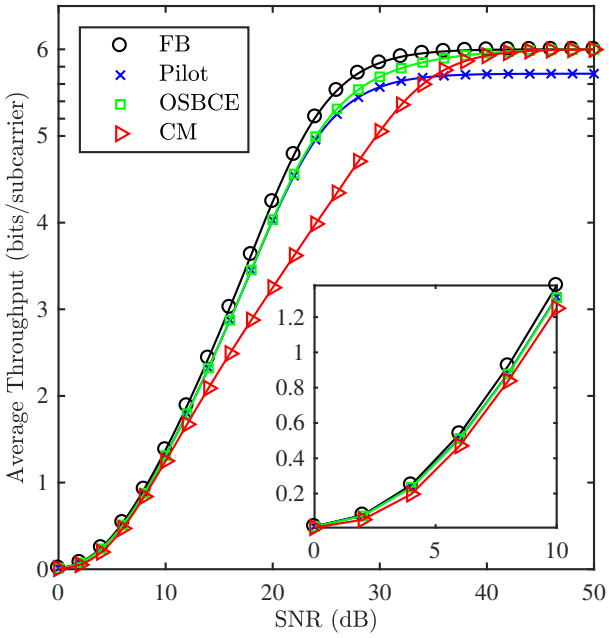

Fig. 15. Average throughput per subcarrier for $P_{th} = 10^{-3}$.

FB system is shown in Fig. 15, where the FB system is used as an upper limit to compare the spectral efficiency of the considered systems. The modulation order for all the considered systems varies from $1 \leq M(\ell, k) \leq 64$, where the Incremental Allocation Algorithm [44] is used to solve the optimization problem in (62). For the pilot-based system, the distribution of the data and pilot subcarriers follows the

LTE-A transmission grid as in Fig. 1a. As it can be noted from Fig. 15, the throughput for all the considered systems is approximately equal for low SNR values, namely for SNR $\lesssim 10$ dB. In the moderate SNR range, $10 \lesssim \mathrm{SNR} \lesssim 25$ dB, it can be noted that the OSBCE and the pilot-based system provide equivalent throughput while the CM throughput is well below the OSBCE and pilot-based systems. At high SNRs, the OSBCE and CM throughput approaches the FB system while the pilot-based saturates at 5.71 bit/subcarrier. Therefore, the OSBCE outperforms the pilot-based and CM for a wide range of SNRs.

It is worth noting that various approaches have been considered in the literature to provide the transmitter with the instantaneous SNRs that are required for applications such as bit loading, beamforming and precoding. Examples for such approaches are channel feedback [45], channel sounding [46] and channel reciprocity [47]. In channel feedback techniques, the channel estimates are obtained at the receiver side, and then fed back to the transmitter. On the contrary, channel sounding and channel reciprocity techniques do not rely on the receiver because the transmitter directly estimates the channel coefficients. Therefore, the optimization processes performed at the transmitter become independent of the channel estimation accuracy at the receiver side if one of the last two techniques is incorporated.

VIII. Conclusion and Future Work

In this work, a novel blind channel estimator was introduced for OFDM systems with single transmit antenna based on a hybrid OFDM symbol structure, where pilot subcarriers in conventional OFDM systems are replaced by MPSK symbols, and the adjacent subcarriers are modulated using MASK. Therefore, the MASK symbol can be considered equivalent to the channel frequency response with respect to the MPSK symbol, and hence, the MPSK symbol can be immediately detected, and then used to estimate the channel in a DD manner. The paper also showed that the proposed OSBCE can be incorporated effectively and efficiently in practical systems such as LTE-A standard. The proposed estimator requires one OFDM symbol to estimate the CFR, which makes it suitable for mobile channels, where the channel frequently varies in the time domain. Monte Carlo simulation was used to verify the analytical results, which also confirmed that the OSBCE can produce reliable channel estimates as compared to pilot-based systems, with similar complexity, but with improved spectral efficiency. In future work, the proposed technique will be extended to the multiple transmit antenna case.

References

[1] E. Dahlman, S. Parkvall and J. Skold, 4G: LTE/LTE-Advanced for Mobile Broadband, Academic Press, 2nd Edition, London, UK, 2013.

[2] Digital Video Broadcasting (DVB); Frame Structure, Channel Coding and Modulation for a Second Generation Digital Terrestrial Television Broadcasting System (DVB-T2), ETSI Standard (EN) 302 755, 2011.

[3] IEEE Standard for Information technology, Telecommunications and information exchange between systems Local and metropolitan area networks, Part 11: Wireless LAN Medium Access Control (MAC) and Physical Layer (PHY) Specifications, IEEE Std. 802.11-2012.

[4] IEEE Standard for Wireless MAN-Advanced Air Interface for Broadband Wireless Access Systems, Std. IEEE 802.16.1-2012.

[5] LTE; Evolved Universal Terrestrial Radio Access (E-UTRA), LTE physical layer, 3GPP TS 36.300, 2011.

[6] H. Lin, "Flexible configured OFDM for 5G air interface," *IEEE Access*, vol. 3, pp. 1861-1870, Sep. 2015.

[7] M. Morelli and U. Mengali, "A comparison of pilot-aided channel estimation methods for OFDM systems," *IEEE Trans. Signal Process.*, vol. 49, no. 12, pp. 3065-3073, Dec. 2001.

[8] Ye Li, "Pilot-symbol-aided channel estimation for OFDM in wireless systems," *IEEE Trans. Veh. Technol.*, vol. 49, no. 4, pp. 1207-1215, July 2000.

[9] W. Chen and C. Chung, "Spectrally efficient OFDM pilot waveform for channel estimation," *IEEE Trans. Commun.*, vol. 65, no. 1, pp. 387-402, Jan. 2017.

[10] X. He, R. Song and W. Zhu, "Pilot allocation for distributed-compressed-sensing-based sparse channel estimation in MIMO-OFDM systems," *IEEE Trans. Veh. Technol*., vol. 65, no. 5, pp. 2990-3004, May 2016.

[11] R. Mohammadian, A. Amini and B. H. Khalaj, "Compressive sensing-based pilot design for sparse channel estimation in OFDM systems," *IEEE Commun. Lett*., vol. 21, no. 1, pp. 4-7, Jan. 2017.

[12] X. Dong, W. Lu and A. Soong, "Linear interpolation in pilot symbol assisted channel estimation for OFDM," *IEEE Trans. Wireless Commun.*, vol. 6, no. 5, pp. 1910-1920, May 2007.

[13] M. X. Chang and T. D. Hsieh, "Detection of OFDM signals in fast-varying channels with low-density pilot symbols," *IEEE Trans. Veh. Technol.,* vol. 57, no. 2, pp. 859-872, Mar. 2008.

[14] C. Qi, G. Yue, L. Wu, Y. Huang and A. Nallanathan, "Pilot design schemes for sparse channel estimation in OFDM systems," *IEEE Trans. Veh. Technol.*, vol. 64, no. 4, pp. 1493-1505, Apr. 2015.

[15] A. Al-Dweik and Y. Iraqi, "Error probability analysis and applications of amplitude-coherent detection in flat Rayleigh fading channels," *IEEE Trans. Commun.,* vol. 64, no. 5, pp. 2235-2244, May 2016.

[16] C. Tu and B. Champagne, "Subspace-based blind channel estimation for MIMO-OFDM systems with reduced time averaging," *IEEE Trans. Veh. Technol.*, vol. 59, no. 3, pp. 1539–1544, Mar. 2010.

[17] F. Gao, Y. Zeng, A. Nallanathan, and T. S. Ng, "Robust subspace blind channel estimation for cyclic prefixed MIMO OFDM systems," *IEEE J. Sel. Areas Commun.*, vol. 26, no. 2, pp. 378–388, Feb. 2008.

[18] M. C. Necker and G. L. Stï¿œber, "Totally blind channel estimation for OFDM on fast varying mobile radio channels," *IEEE Trans. Wireless Commun.*, vol. 3, no. 5, pp. 1514–1525, Sep. 2004.

[19] F. Gao and A. Nallanathan, "Blind channel estimation for MIMO OFDM systems via non redundant linear precoding," *IEEE Trans. Signal Process.*, vol. 55, no. 2, pp. 784–789, Feb. 2007.

[20] T. Al-Naffouri, A. Dahman, M. Sohail, W. Xu and B. Hassibi, "Low-complexity blind equalization for OFDM systems with general constellations," *IEEE Trans. Signal Process.*, vol. 60, no. 12, pp. 6395-6407, Dec. 2012.

[21] S. Banani and R. Vaughan, "OFDM with iterative blind channel estimation," *IEEE Trans. Veh. Technol.*, vol. 59, no. 9, Nov. 2010.

[22] S. Park, B. Shim and J. Choi, "Iterative channel estimation using virtual pilot signals for MIMO-OFDM systems," *IEEE Trans. Signal Process.,* vol. 63, no. 12, pp. 3032-3045, June 2015.

[23] M. Song, D. Kim and G. Im, "Recursive channel estimation method for OFDM-based cooperative systems," *IEEE Commun. Lett*., vol. 14, no. 11, pp. 1029-1031, Nov. 2010.

[24] Tao Cui and C. Tellambura, "Joint data detection and channel estimation for OFDM systems," *IEEE Trans. Commun.*, vol. 54, no. 4, pp. 670-679, Apr. 2006.

[25] M. Muck, M. de Courville and P. Duhamel, "A pseudorandom postfix OFDM modulator - semi-blind channel estimation and equalization," *IEEE Trans. Signal Process.*, vol. 54, no. 3, pp. 1005-1017, Mar. 2006.

[26] S. Abdallah and I. Psaromiligkos, "Semi-blind channel estimation with superimposed training for OFDM-based AF two-way relaying," *IEEE Trans. Wireless Commun.*, vol. 13, no. 5, pp. 2468-2467, May 2014.

[27] Ming-Xian Chang and Y. T. Su, "Performance analysis of equalized OFDM systems in Rayleigh fading," *IEEE Trans. Wireless Commun.*, vol. 1, no. 4, pp. 721-732, Oct. 2002.

[28] A. Al-Dweik, A. Hazmi, S. Younis, B. Sharif, and C. Tsimenidis, "Carrier frequency offset estimation for OFDM systems over mobile Radio channels," *IEEE Trans. Veh. Technol.*, vol. 59, pp. 974-979, Feb. 2010.

[29] M. Mirahmadi, A. Al-Dweik and A. Shami, "BER reduction of OFDM based broadband communication systems over multipath channels with impulsive noise," *IEEE Trans. Commun.*,vol. 61, no. 11, pp. 4602-4615, Nov. 2013.

[30] M. S. Ahmed, S. Boussakta, B. S. Sharif and C. C. Tsimenidis, "OFDM based on low complexity transform to increase multipath resilience and reduce PAPR," *IEEE Trans. Signal Process.*, vol. 59, no. 12, pp. 5994-6007, Dec. 2011.
[31] S. Tomasin and M. Butussi, "Analysis of interpolated channel estimation for mobile OFDM systems," *IEEE Trans. Commun.* vol. 58, no. 5, pp. 1578-1588, May 2010.
[32] F. D'Agostini, S. Carboni, M. De Castro, F. De Castro, and D. Trindade, "Adaptive concurrent equalization applied to multicarrier OFDM systems," *IEEE Trans. Broadcast.,* vol. 54, no. 3, pp. 441-447, Sep. 2008.
[33] M. Henkel, C. Schilling and W. Schroer, "Comparison of channel estimation methods for pilot aided OFDM systems," in *Proc. IEEE VTC. Spring,* Dublin, 2007, pp. 1435-1439.
[34] S. Liu, F. Wang, R. Zhang and Y. Liu, "A simplified parametric channel estimation scheme for OFDM systems," *IEEE Trans. Wireless Commun.*, vol. 7, no. 12, pp. 5082-5090, Dec. 2008.
[35] M. Chang, "A new derivation of least-squares-fitting principle for OFDM channel estimation," *IEEE Trans. Wireless Commun.*, vol. 5, no. 4, pp. 726-731, Apr. 2006.
[36] M. K. Simon, S. M. Hinedi, and W. C. Lindsey, *Digital communication techniques: signal design and detection*, Prentice Hall PTR, 1995.
[37] J. G. Proakis, and M. Salehi, *Digital communications*, 4th ed. New York: McGraw-Hill, 2001.
[38] M. K. Simon and M. S. Alouini, *Digital Communication over Fading Channels–A Unified Approach to Performance Analysis*, 2nd Ed., Wiley, 2005.
[39] M. Kalil, A. Shami, A. Al-Dweik, and S. Muhaidat, "Low-complexity power-efficient schedulers for LTE uplink with delay-sensitive traffic," *IEEE Trans. Veh. Technol*, vol. 64, no. 10, pp. 4551-4564, Oct. 2015.
[40] ETSI TR 125 943 V9.0.0 (2010-02), Universal Mobile Telecommunications System (UMTS) Deployment Aspects, 3GPP TR 25.943, Release 9.
[41] R. Mallik and N. Sagias, "Distribution of inner product of complex Gaussian random vectors and its applications," *IEEE Trans. Commun.*, vol. 59, no. 12, pp. 3353-3362, Dec. 2011.
[42] F. Xiong, "M-ary amplitude shift keying OFDM system," *IEEE Trans. Commun.,* vol. 51, no. 10, pp. 1638-1642, Oct. 2003.
[43] C. H. Tseng, Y. C. Cheng and C. D. Chung, "Subspace-based blind channel estimation for OFDM by exploiting cyclic prefix," *IEEE Wireless Commun. Lett*., vol. 2, no. 6, pp. 691-694, Dec. 2013.
[44] A. Wyglinski, F. Labeau, and P. Kabal, "Bit loading with BER-constraint for multicarrier systems," *IEEE Trans. Wireless Commun.*, vol. 4, no. 4, pp. 1383-1387, July 2005.
[45] A. Alkhateeb and R. W. Heath, "Frequency selective hybrid precoding for limited feedback millimeter wave systems," *IEEE Trans. Commun.,* vol. 64, no. 5, pp. 1801-1818, May 2016.
[46] N. B. Mehta, S. Kashyap and A. F. Molisch, "Antenna selection in LTE: from motivation to specification," *IEEE Commun. Mag.,* vol. 50, no. 10, pp. 144-150, Oct. 2012.
[47] F. E. Dorcheh and S. Shahbazpanahi, "Jointly optimal pre- and post-channel equalization and distributed beamforming in asynchronous bidirectional relay networks," *IEEE Trans. Signal Process.*, vol. 65, no. 17, pp. 4593-4608, Sept. 2017.

Anas Saci (S'15) received his B.Sc. degree from Jordan University of Science and Technology, Jordan, and the M.Sc. degree from Télécom ParisTech, France in 2013 and 2015, respectively. He is currently pursuing a Ph.D. in Electrical and Computer Engineering at the University of Western Ontario, London, Canada. His research interest includes wireless communications, OFDM systems, and channel estimation.

Arafat Al-Dweik (S'97 - M'01 - SM'04) received the B.Sc. degree in Telecommunication Engineering from Yarmouk University, Jordan, in 1994 and the M.S. (*Summa Cum Laude*) and Ph.D. (*Magna Cum Laude*) degrees in electrical engineering from Cleveland State University, Cleveland, OH, USA in 1998 and 2001, respectively. He was with Efficient Channel Coding, Inc., Cleveland-Ohio, from 1999 to 2001, where he was a Research and Development Engineer working on advanced modulation, coding, and synchronization techniques. From 2001 to 2003, he was the Head of Department of Information Technology at the Arab American University in Palestine. From 2003 to 2012, he was with the Communications Engineering Department, Khalifa University, United Arab Emirates. He joined University of Guelph, ON, Canada, as an Associate Professor from 2013-2014. Dr. Al-Dweik is a Visiting Research Fellow at the School of Electrical, Electronic and Computer Engineering, Newcastle University, Newcastle upon Tyne, UK since 2006 till present. He is also a Research Professor and member of the School of Graduate Studies at Western University, London, ON, Canada. Dr Al-Dweik has extensive editorial experience where he serves as an Associate Editor at the IEEE TRANSACTIONS ON VEHICULAR TECHNOLOGY and *IET Communications*. Moreover, he was a TPC member in several major conferences such as the IEEE GLOBECOM, ICC, PIMRC and WCNC. Dr Al-Dweik have received several research awards and he is a recipient of the Fulbright Scholarship.

Abdallah Shami (SM'09) received the B.E. degree in electrical and computer engineering from the Lebanese University, Beirut, Lebanon, in 1997 and the Ph.D. degree in electrical engineering from the City University of New York, New York, NY, USA in 2002.

Since July 2004, he has been with the University of Western Ontario, London, ON, Canada, where he is currently a Professor with the Department of Electrical and Computer Engineering. His current research interests include network-based cloud computing and wireless/data networking.

Dr. Shami is the Chair of the IEEE Communications Society Technical Committee on Communications Software. He has served as the Chair for the key symposia of the IEEE Global Communications Conference; the IEEE International Conference on Communications; the IEEE International Conference on Computing, Networking, and Communications; and the International Conference on Computer and Information Technology. He currently serves as an Associate Editor for IEEE COMMUNICATIONS SURVEY AND TUTORIALS, *IET Communications Journal*, and the *Wiley Journal of Wireless Communications and Mobile Computing*.

Youssef Iraqi (S'98 - M'03 - SM'10) is an Associate Professor at Khalifa University, UAE. He received his M.Sc. and Ph.D. degrees in Computer Science from the University of Montreal, Canada, in 2000 and 2003 respectively. Y. Iraqi has published more than 80 research papers in international journals and conference proceedings. In 2008, he received the IEEE Communications Society Fred W. Ellersick prize. He is a senior member of the IEEE. His research interests include resource management in distributed environments and wireless networking.